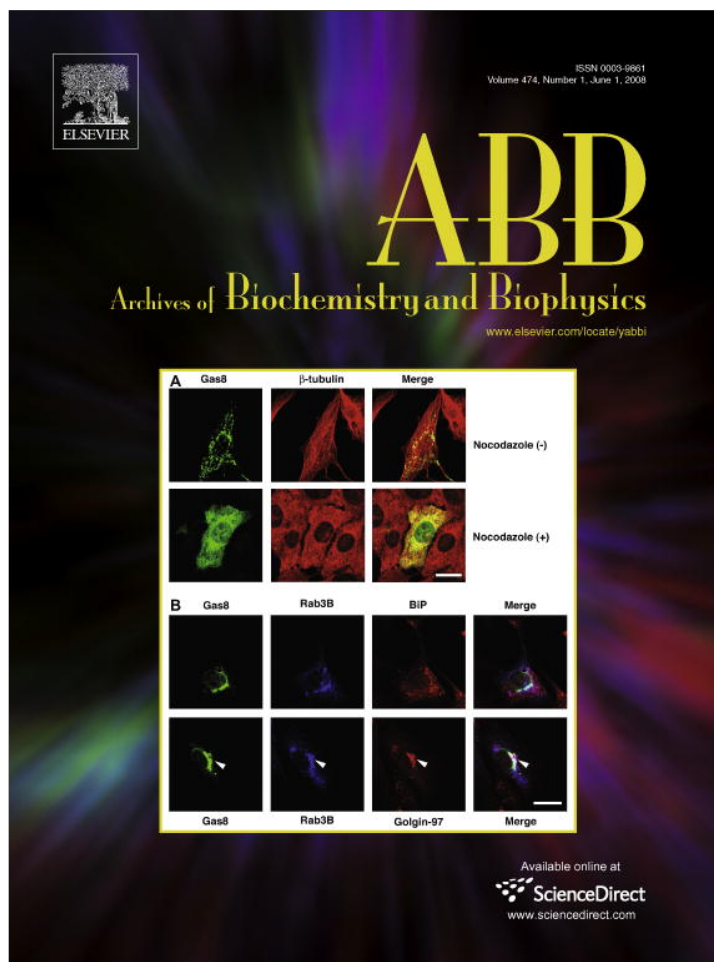


Provided for non-commercial research and education use.
Not for reproduction, distribution or commercial use.



This article appeared in a journal published by Elsevier. The attached copy is furnished to the author for internal non-commercial research and education use, including for instruction at the authors institution and sharing with colleagues.

Other uses, including reproduction and distribution, or selling or licensing copies, or posting to personal, institutional or third party websites are prohibited.

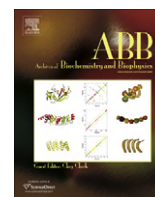
In most cases authors are permitted to post their version of the article (e.g. in Word or Tex form) to their personal website or institutional repository. Authors requiring further information regarding Elsevier's archiving and manuscript policies are encouraged to visit:

<http://www.elsevier.com/copyright>



Contents lists available at ScienceDirect

Archives of Biochemistry and Biophysics

journal homepage: www.elsevier.com/locate/yabbi

Structure of the two-subsite β -D-xylosidase from *Selenomonas ruminantium* in complex with 1,3-bis[tris(hydroxymethyl)methylamino]propane[☆]

Joseph S. Brunzelle^a, Douglas B. Jordan^{b,*}, Darrell R. McCaslin^c, Andrzej Olczak^d, Zdzislaw Wawrzak^e^a Northwestern University Center for Synchrotron Research, Life Sciences Collaborative Access Team, Department of Molecular Pharmacology and Biological Chemistry, 9700 South Cass Avenue, Argonne, IL 60439, USA^b Fermentation Biotechnology Research Unit, National Center for Agricultural Utilization Research, U.S. Department of Agriculture, Agricultural Research Service, 1815 North University Street, Peoria, IL 61604, USA^c Department of Biochemistry, Biophysics Instrumentation Facility, 433 Babcock Drive, University of Wisconsin-Madison, Madison, WI 53706-1544, USA^d Institute of General and Ecological Chemistry, Technical University of Lodz, ul. Zeromskiego 116, 90-924 Lodz, Poland^e Department of Biochemistry, Molecular Biology and Cell Biology, Northwestern University, 2205 Tech Drive, Evanston, IL 60208-3500, USA

ARTICLE INFO

Article history:

Received 29 January 2008
and in revised form 5 March 2008
Available online 14 March 2008

Keywords:

Glycoside hydrolase
GH43
 α -L-Arabinofuranosidase
Structure-function
Protein crystallography
Sedimentation equilibrium

ABSTRACT

The three-dimensional structure of the catalytically efficient β -xylosidase from *Selenomonas ruminantium* in complex with competitive inhibitor 1,3-bis[tris(hydroxymethyl)methylamino]propane (BTP) was determined by using X-ray crystallography (1.3 Å resolution). Most H bonds between inhibitor and protein occur within subsite –1, including one between the carboxyl group of E186 and an N group of BTP. The other N of BTP occupies subsite +1 near K99. E186 (pK_a 7.2) serves as catalytic acid. The pH (6–10) profile for $1/K_i^{(BTP)}$ is bell-shaped with pK_a's 6.8 and 7.8 on the acidic limb assigned to E186 and inhibitor groups and 9.9 on the basic limb assigned to inhibitor. Mutation K99A eliminates pK_a 7.8, strongly suggesting that the BTP monocation binds to the dianionic enzyme D14[–]E186[–]. A sedimentation equilibrium experiment estimates a K_d ($[\text{dimer}]^2/[\text{tetramer}]$) of 7×10^{-9} M. Similar k_{cat} and k_{cat}/K_m values were determined when the tetramer/dimer ratio changes from 0.0028 to 26 suggesting that dimers and tetramers are equally active forms.

© 2008 Elsevier Inc. All rights reserved.

β -D-Xylosidase/ α -L-arabinofuranosidase from *Selenomonas ruminantium* (SXA)¹, a family 43 glycoside hydrolase (GH43), is the best catalyst known for promoting the hydrolysis of 1,4- β -xylooligosaccharides [1,2]. By having the highest known k_{cat} and k_{cat}/K_m values with xylooligosaccharide substrates, bifunctionality of β -xylosidase (EC 3.2.1.37) and α -arabinofuranosidase (EC 3.2.1.55) activities [1–5], and good thermal and pH stabilities [5], SXA has potential utility in industrial processes for saccharification of herbaceous biomass (arabinoxylan fraction) to simple sugars that can be fermented to ethanol and other products [6,7].

A common structural feature of enzymes belonging to glycoside hydrolase families 32, 43, 62, and 68 is a 5-bladed β -propeller domain that comprises the catalytic acid and the catalytic base [8–10]. Recently-determined X-ray structures of GH43 β -xylosidases from *Bacillus subtilis*, *Bacillus halodurans*, *Clostridium acetobutylicum*, and *Geobacillus stearothermophilus*, which have 53–70% protein sequence identity with SXA, show that the enzymes possess an additional C-terminal β -sandwich domain that serves to close off a portion of the active site to form a pocket. The active-site pocket comprises two subsites (binding capacity for two monosaccharide moieties) and a single route of access for small molecules such as substrate. The additional residues of oligosaccharide substrates, comprising more than two monosaccharide residues, must extend the additional residues beyond subsite +1 of the active-site pocket to bulk solvent [1,3,8]. The structure of a catalytically inactive, site-directed mutant of *G. stearothermophilus* β -xylosidase (PDB ID 2EXK; containing E187G mutation of catalytic acid) in complex with β -1,4-xylobiose [8] has been most useful in modeling the SXA active site. Complementary to the structural information, biochemical studies have established that (a) SXA catalyzes hydrolysis of 4NPX and β -1,4-xylobiose with inversion of stereochemistry implicating a single transition state

[☆] Atomic coordinates and structure factors for β -D-xylosidase from *Selenomonas ruminantium* in complex with 1,3-bis[tris(hydroxymethyl)methylamino]propane have been deposited in the Research Collaboratory for Structural Bioinformatics (<http://www.rcsb.org/pdb>) with the accession code 3C2U.

* Corresponding author. Fax: +1 309 681 6427.

E-mail address: douglas.jordan@ars.usda.gov (D.B. Jordan).

¹ Abbreviations used: SXA, β -D-xylosidase/ α -L-arabinofuranosidase from *S. ruminantium*; 4NPX, 4-nitrophenyl- β -D-xylopyranoside; 4NPA, 4-nitrophenyl- α -L-arabinofuranoside; GH, glycoside hydrolase; GH43, glycoside hydrolase family 43; BTP, 1,3-bis[tris(hydroxymethyl)methylamino]propane; SAS, solvent accessible surface; rms, root mean squared; M_w , weight-average molecular weight; M_s , sequence molecular weight.

with the catalytic base (D14) serving to activate a water molecule for addition to substrate and the catalytic acid (E186) serving to protonate the leaving group, (b) SXA catalyzes the hydrolysis of a single residue from the nonreducing end of substrate without processivity so that all products of the hydrolysis reaction are removed from the active site before initiating another catalytic cycle [1], (c) the single active site of the SXA protomer is responsible for both the β -xylosidase and α -arabinofuranosidase activities [1,4], and (d) catalysis is governed by pK_a 5.0 and pK_a 7.2, respectively, assigned to the catalytic base, D14, and the catalytic acid, E186, such that SXA in the D14^HE186^H form is catalytically active and SXA in the D14^HE186^H and D14^HE186⁻ forms are catalytically inactive [1,3]. pK_a values of the three active-site carboxylic acid residues (D14, D127, and E186) are likely raised by their proximity to one another (within 6 Å); pK_a 5.0, reporting the carboxyl group of D14, is likely made more normal by its close proximity (4.2 Å) to the guanidinium group of R290 and pK_a 7.2, reporting the carboxyl group of E186, is likely made more basic by its close proximity (3.8 Å) to the carboxyl group of D127 [1].

In addition to controlling catalysis, the protonation state of D14 and E186 controls the affinity of SXA for inhibitory monosaccharides, whereas D14^HE186^H has no binding affinity for monosaccharides, D14^HE186^H and D14^HE186⁻ enzyme forms are capable of binding monosaccharides and the preference for one or the other enzyme forms is monosaccharide dependent [3]. Only D14^HE186^H SXA is capable of binding two equivalents of monosaccharide per active site. We have proposed that the negatively charged environment that is confined mostly within subsite -1 of D14^HE186⁻ repels binding of monosaccharides therein and leaves subsite +1 open for binding of a single monosaccharide per active site [3].

None of the saccharide inhibitors has been found to bind only to the D14^HE186⁻ form of SXA, and such ligands would be useful in analyzing binding modes of GH43 β -xylosidases. Aminoalcohols could serve this purpose because subsite -1 of SXA is occupied by one glutamic and two aspartic residues that offer potential recognition elements for cations (coulombic interactions). Active-site carboxyl groups have been observed in near proximity to the amino group of tris(hydroxymethyl)aminomethane (Tris) [11,12] and the N group of iminosugars in X-ray structures of other glycoside hydrolases in complex with Tris and iminosugars [13–15]. One of the latter structures has high enough resolution to assign two hydrogen substituents to the imine of an iminosugar to define its cationic state and to assign bond lengths of glutamyl carboxyl groups as deprotonated and anionic for forming favorable electrostatic interactions with the cationic N [15]. For this work, we determined the X-ray structure of SXA in complex with an aminoalcohol and biochemically characterized the binding properties. This constitutes the first structure of a native GH43 β -xylosidase in complex with an active-site ligand. Also, we determined the dissociation constant for the SXA homotetramer to its dimers from a sedimentation equilibrium experiment and established that both enzyme forms have similar catalytic properties.

Materials and methods

Materials and general methods

4NPX, BTP, inhibitor candidates, and buffers were obtained from Sigma-Aldrich. Water was purified through a Milli-Q unit (Millipore). All other reagents were reagent grade and high purity. A Cary 50 Bio UV-Visible spectrophotometer (Varian), equipped with a thermostatted holder for cuvettes, was used for spectral and kinetic determinations. A model SX.18MV-R stopped-flow (Applied Photophysics), with a thermostatted compartment for syringes and reaction chamber and a 2 mm path length for absorbance measurements, was used for rapid kinetic studies. An AVIV Model 215 circular dichroism spectrophotometer (Aviv Biomedical), equipped with thermostatted cuvette holder, and a 1 mm path length quartz cuvette were used for acquiring protein spectra; three spectra were averaged for each protein sample. Manipulations of coordinates (overlays, distance measurements,

calculations of solvent accessible surfaces, etc.) and molecular graphics images were through the UCSF Chimera package from the Resource of Biocomputing, Visualization, and Informatics at the University of California, San Francisco (supported by NIH P41 RR-01081) [16].

Protein preparations

Site-directed mutagenesis was performed as described [1,4]. Oligonucleotide primers for the K99A mutant were 5'-GGTCGTAGACGGCATGTGGGCGGATTGTCATAACTACCTG-3' and 5'-CAGGTAGTTATGACAATCCGCCACATGCCGCTACGACC-3'; the template was pSRA1 with the SXA gene cloned into pET21(+) [17]. BL21(DE3) cells producing SXA or SXA K99A mutant were grown and induced as described [1]. BL21(DE3) cells producing selenomethionine-containing SXA were grown similarly with the exceptions that defined media including selenomethionine [18] was used, cells were grown at 25–30 °C and expression of the SXA gene was induced with 1 mM isopropyl- β -D-thiogalactopyranoside for 16 h prior to cell harvest. SXA proteins were purified to homogeneity (judged by SDS-PAGE analysis) as described [1], with the addition of a final desalting, gel filtration step employing a 2.6 \times 30 cm column of Bio-Gel P-6 DG desalting gel (Bio-Rad), equilibrated and developed with 20 mM sodium phosphate, pH 7.3. K99A SXA and selenomethionine-containing SXA behaved similarly to wild-type SXA in terms of high yields in *Escherichia coli* (~30% of soluble protein) and elution times from chromatography columns. Circular dichroism spectra (190–260 nm, collected for samples containing 8 μ M enzyme in 20 mM sodium phosphate, pH 7.3) are characterized by a major trough at 214 nm (reflecting dominance of β structure), and the spectra are similar for wild-type SXA and the K99A SXA: mean trough value $[\theta]$ at 214 nm for two wild-type SXA samples = $(-2.97 \pm 0.14) \times 10^6$ deg cm² dmol⁻¹; trough value $[\theta]$ at 214 nm for the K99A mutant = -2.87×10^6 deg cm² dmol⁻¹.

Crystallization and structure determination

Native and selenomethionine-containing crystals of β -D-xylosidase from *S. ruminantium* were obtained from drops containing 4 μ L of protein solution (1.6 mg/mL in 0.1 M BTP-HCl, pH 8.0) mixed with 1 μ L of the well solution containing 22–25% (w/v) PEG 1100 monomethyl ether in 0.1 M BTP-HCl, pH 8.0. After about one week of growth, suitable crystals were harvested and flash frozen in liquid nitrogen. Multi-wavelength anomalous dispersive (MAD) data, collected at the selenium peak, edge, and high energy remote, and native data were collected using a MARMOSAIC 225 CCD detector (MarResearch) at the DuPont-Northwestern-Dow (DND) beamline, Sector 5 ID-B of the Advance Photon Source (Argonne, IL). Anomalous diffraction data were processed and scaled using XGEN [19], and native diffraction data were processed and scaled using XDS [20]. Native and selenomethionine-containing crystals are of the same triclinic space group P1 with a homotetramer in the asymmetric unit.

Shake-n-Bake [21] was used to find 28 of 32 possible selenium sites. The initial sites were refined, and initial phases were calculated with MLPHARE [22]. Initial phases, with an overall figure of merit of 0.301, were improved by solvent flattening, phase extension, and 4-fold non-crystallographic symmetry (NCS) averaging, and provided an interpretable electron density map with an overall figure of merit of 0.653 using DM [23]. Automatic model building with ARP/wARP [24] aided with the program Xfit from XtalView [25] correctly built ~95% of the protein. The remaining model was traced manually with COOT [26] alternated with positional refinement against the 1.3 Å native data set using REFMAC5 [27]. Solvent molecules were added with ARP/wARP and alternative positions were added manually and refined with REFMAC5.

Enzyme-catalyzed reactions

Unless indicated otherwise, reactions were initiated by adding a small aliquot of enzyme (generally 7 μ L of enzyme diluted into 10 mM sodium phosphate, pH 7.0, and incubated on wet ice or at ~25 °C) to 1-mL temperature-equilibrated (25 °C) reaction mixtures, which were monitored continuously (Cary spectrophotometer) for 0.3 min at 380 nm (for pH values below 6) or 400 nm (for pH values of 6 and above) for determinations of linear initial rates (steady-state rates). Time required for enzyme addition and mixing was 0.2 min prior to collection of rate data. With 4NPA and 4NPX as substrates, initial rates determined from 0.1-s (using stopped-flow instrument) and 30-min reactions were similar [1]. Delta extinction coefficients (product-substrate) used for molar conversion calculations for each reaction condition and end point determinations of 4NPA and 4NPX substrate concentrations were determined as described [1]. Buffers of constant ionic strength ($I = 0.3$ M), adjusted with NaCl, in the complete reaction mixtures were used as indicated: 100 mM succinate-NaOH (pH 4.3–6), 100 mM sodium phosphate (pH 6–8), 30 mM sodium pyrophosphate (pH 8–10). Discontinuous monitoring of reaction progress for determination of initial rates was conducted as described [1,4]. Values for v and k_{cat} are expressed in moles substrate hydrolyzed per second per mole of enzyme active sites (protomers), the latter determined using the calculated extinction coefficient of SXA protomers at 280 nm of 129600 M⁻¹ cm⁻¹ [1,28].

Sedimentation equilibrium centrifugation

A sedimentation equilibrium experiment was performed in a Beckman XL-A analytical ultracentrifuge using double-sector, 1.2 cm pathlength, charcoal-filled epon centerpieces and described methods [29]. All data were collected at 4 °C and the protein gradient was monitored at 278 nm. Three samples were prepared by diluting a 0.292 mM SXA stock solution (protomer concentration) with buffer P (100 mM sodium phosphate, pH 7.0) to give initial absorbances as measured in the centrifuge of 0.688, 0.436 and 0.252. Depletion of the protein at the end of the experiment gave non-sedimenting absorbances of –0.001, 0.006, and 0.002, respectively. Approximately 100 μ L of sample was placed in one sector and ~107 μ L of buffer P in the other sector as reference. The samples were allowed to equilibrate at 3000, 4700, 6200, 7800, and 10000 rpm taking superimposable gradients recorded 2–4 h apart as demonstrating equilibrium. After recording the 10000 rpm data and as a check for irreversible aggregation, the sample was allowed to re-equilibrate at 6200 rpm. These gradients were essentially superimposable with the initial 6200 rpm data, demonstrating that large irreversible aggregates did not form during the experiment.

Data evaluation involved global fitting of the absorbance data sets versus squared radial distance from the center of rotation (r^2) to various models (explicit equations) in an approach similar to that of Laue [29] using programs written for Igor Pro (Wavemetrics, Lake Oswego, OR). Fitted parameters included one or two reduced molecular weights ($M_w(1 - \bar{v}\rho)$) with the implicit assumption that all species have the same absorbance per unit mass and partial specific volume. M_w is a weight average molecular weight; \bar{v} is the partial specific volume, calculated based on the SXA amino acid composition as 0.731 mL/g; and ρ is the density of buffer P, measured at 4 °C using an Anton-Paar DMA 5000 density meter to be 1.01295 g/mL. A concentration for each independent species was fit at a reference position (chosen as 49.4 cm²); for the model with two species in equilibrium, the concentration of the smaller species at the reference position was fitted. The molecular weight of the SXA polypeptide chain is 61137 (M_s).

Equations

Data were fitted to Eqs. (1)–(7) using the computer program Graftit (Erithacus Software) [30]. Simple weighting (constant error) was used for fitting most data; proportional error weighting was used to fit some data (e.g., certain pH curves). For Eqs. 1 and 2, v is the observed initial (steady-state) rate of catalysis, k_{cat} is the maximum rate of catalysis, S is the substrate concentration, K_m is the Michaelis constant, I is the inhibitor concentration and K_i is the competitive inhibition constant. For Eqs. 3, 7, p is the determined parameter at a single pH, P is the pH-independent value of the parameter, H^+ is the proton concentration, K_{a1} is the acid dissociation constant of the first group affecting P , K_{a2} is the acid dissociation constant of the second group affecting P , K_{a3} is the acid dissociation constant of the third group affecting P , $K_{a(enz)}$ is the acid dissociation constant of the enzyme group affecting P , $K_{a1(inh)}$ is the acid dissociation constant of the first inhibitor group affecting P , $K_{a2(inh)}$ is the acid dissociation constant of the second inhibitor group affecting P , $K_{a(inh)}$ is the acid dissociation constant of the inhibitor group affecting P , $K_{a1(enz)}$ is the acid dissociation constant of the first enzyme group affecting P , and $K_{a2(enz)}$ is the acid dissociation constant of the second enzyme group affecting P .

$$v = \frac{k_{cat} * S}{K_m + S} \quad (1)$$

$$v = \frac{k_{cat} * S}{K_m \left(1 + \frac{I}{K_i}\right) + S} \quad (2)$$

$$p = \frac{P}{1 + \frac{H^+}{K_{a1}} * \frac{H^+}{K_{a2}} + \frac{H^+}{K_{a2}} + \frac{K_{a3}}{H^+}} \quad (3)$$

$$p = \frac{P}{1 + \frac{H^+}{K_{a1}} + \frac{K_{a3}}{H^+}} \quad (4)$$

$$p = \frac{P}{\left(1 + \frac{H^+}{K_{a(enz)}}\right) * \left(1 + \frac{H^+}{K_{a1(inh)}} + \frac{K_{a2(inh)}}{H^+}\right)} \quad (5)$$

$$p = \frac{P}{\left(1 + \frac{H^+}{K_{a(enz)}}\right) * \left(1 + \frac{K_{a(inh)}}{H^+}\right)} \quad (6)$$

$$p = \frac{P}{\left(1 + \frac{H^+}{K_{a1(enz)}} * \frac{H^+}{K_{a2(enz)}} + \frac{H^+}{K_{a2(enz)}}\right) * \left(1 + \frac{K_{a1(inh)}}{H^+}\right)} \quad (7)$$

Results and discussion

SXA structure and comparisons with other GH43 β -xylosidases

The three-dimensional structure of SXA was solved by using MAD phasing methods and X-ray data collected on three crystals of selenomethionine-substituted enzyme. The structure was re-

fined to a R_{work} of 13.4% and an R_{free} of 16.3% using X-ray data extending to 1.30 Å resolution from a single crystal of native SXA. Selenomethionine and native SXA crystals were grown at pH 8.0 in the presence of aminoalcohol inhibitor, 1,3-bis [tris(hydroxymethyl)methylamino]propane (BTP), with 22–25% (w/v) polyethylene glycol 1100 monomethyl ether as the precipitate. In the refined structure, electron density is sufficient for assignments of all 538 amino acid residues of subunit A and the first 537 residues from subunits B, C and D of the SXA tetramer and one BTP per active site (Fig. 1). Additional data collection and refinement statistics are listed in Table 1.

The asymmetric unit comprises a single homotetramer of SXA protomers. Individual overlays of subunits B, C, and D upon subunit A provide an average root mean square (rms) deviation of 0.17 ± 0.01 Å between coordinates of $C\alpha$ atoms, indicating the high degree of structural similarity among the protomers. As well, SXA shares close structural similarity with other GH43 β -xylosidases for which X-ray structures are available (Table 2). GH43 β -xylosidases from *C. acetobutylicum*, *B. subtilis*, *B. halodurans*, and *G. stearothermophilus* are, respectively, 70, 64, 53, and 61% identical to SXA in amino acid sequence. Overlays of individual subunits upon subunit A of SXA provide rms deviations for $C\alpha$ atoms (average of the 2 or 4 subunits in asymmetric units) of 0.51, 0.62, 0.86, and 0.65 Å, respectively, for the other four enzymes. There are 21 amino acid residues [4] within 5 Å of the β -xylobiose residue in the active site of the *G. stearothermophilus* enzyme [8]. Of these, 18 are identical to SXA among the four GH43 β -xylosidases (Table 2), and an overlay of the four structures upon the SXA structure indicates close correspondence of the positions of active-site residues (Fig. 2).

The tetramer of SXA and the other GH43 β -xylosidases exhibits 222 (D_2) symmetry with the A + B dimer turned at 90° against the C + D dimer (Fig. 3). Calculations of solvent accessible surfaces (SAS) indicate that, for SXA, in formation of the two dimers (comprising subunits A + B and C + D) from the tetramer, an additional 4.1×10^3 Å² (or 5.8%) is exposed and that in formation of four protomers from two dimers, an additional 7.9×10^3 Å² (or 10.5%) is exposed, thus indicating that the monomers are held together by more contacts within the dimers than the dimers are held together within the tetramer. Similar SAS values are calculated for the other β -xylosidases (Table 2).

Homotetramer dissociation

Clearly, from the SAS values of the X-ray structures and from inspection, the homotetramers of SXA and its GH43 β -xylosidase counterparts are dimers of dimers (Fig. 3). Gel filtration chromatography has been used to estimate a Stokes radius consistent with a homotetramer for SXA when its concentration was ~10 μ M protomer [5] and a homotrimer for *G. stearothermophilus* at an unspecified concentration [8]. The more accurate method of sedimentation equilibrium ultracentrifugation was used to determine the quaternary state of SXA protomers and its equilibrium constant at pH 7.0 and 4 °C.

Plots of log absorbance versus squared radial position (r^2) show nonlinearity (Fig. 4); and the nonlinearity, more obvious in the higher speed data, suggests the presence of multiple species of SXA. The fit of the data to a single-species model is poor and provides a ratio M_w/M_s of 3.6, again suggestive of multiple species. The data fit a model with two independent, non-equilibrating species very well (the lowest sum of squared residuals of the three models examined) and provides M_w/M_s values for the two species of 2.1 ± 0.1 and 3.95 ± 0.04 , strongly suggesting that the data are adequately described as a mixture of dimers and tetramers. When the larger species is assumed to be twice the M_w of the smaller, the smaller species has M_w/M_s value of 1.96 ± 0.01 . Based on integrated recover-

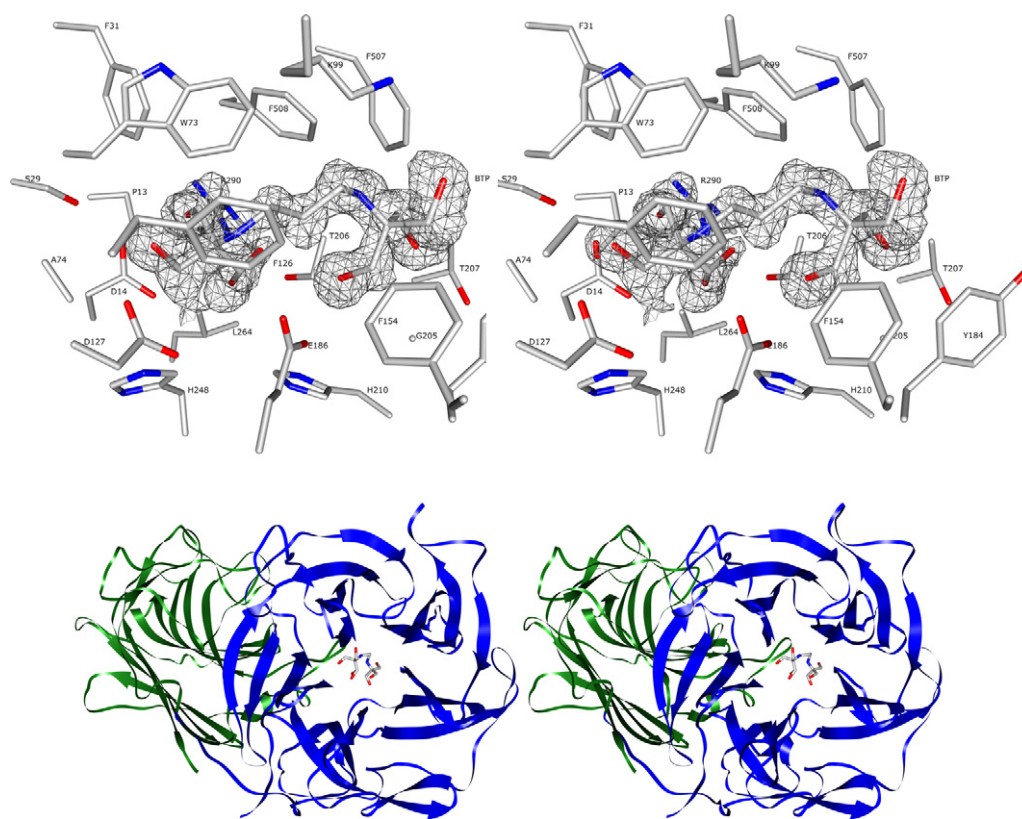


Fig. 1. 1,3-Bis[tris(hydroxymethyl)methylamino]propane (BTP) bound to SXA. Top, stereoview of the SXA active site. The omit map for BTP is contoured at 1.0σ . Bottom, stereoview of the SXA monomer. The N-terminal residues, containing the 5-bladed β -propeller domain, are in the darker color. The C-terminal residues are in the lighter color. BTP is colored by atom type.

ies for the independent species model, the tetramer of SXA was the dominant species in the experiment. Thus, the data strongly point to a mixture of SXA tetramers and SXA dimers. Modeling the data as an equilibrium between two species and restricting the aggregation number to 2, provides a M_w/M_s value of 1.88 ± 0.01 (94% of theoretical) for the dimer and a K_d value ($[\text{dimer}]^2/[\text{tetramer}]$) of $(7.1 \pm 2.5) \times 10^{-9}$ M. Better determination of the dissociation constant requires analysis of significantly lower concentrations of SXA in the cells; the latter requires more sensitive means for monitoring SXA concentrations in the sedimentation gradient.

When *S. ruminantium* cells are grown in media containing xylose or xylooligosaccharides, the reported specific activity of SXA in the crude bacterial extracts is ~ 15 μmol 4NPX hydrolyzed per hour per mg protein at pH 6.8 and 37°C [17]. Under similar reaction conditions (4NPX = 9 mM), homogeneous SXA activity is 6000 μmol 4NPX hydrolyzed per hour per mg protein. So, it can be estimated that 0.25% of the soluble protein in the induced *S. ruminantium* cells is SXA. Assuming that the intracellular protein concentration is 100 mg/mL the concentration of SXA is 4 μM on a protomer basis, and the ratio of tetramer to dimer is 16; the latter value is based on the tetramer–dimer K_d .

The affinity of SXA dimers for one another suggests that the relative concentrations of dimers and tetramers are significant under most experimental conditions. Steady-state kinetic parameters were estimated from initial-rate data determined from reactions containing 40 pM to 10 μM SXA protomer at pH 7.0 and 25°C and monitored for 0.1 s to 20 min. The $[\text{tetramer}]/[\text{dimer}]$ ratio changed from 0.0028 to 26, yet the k_{cat} and k_{cat}/K_m values are similar for the varied reaction conditions (Fig. 5). It is concluded that the dimer and tetramer forms of SXA have similar kinetic properties, which is consistent with the structural information that indicates active sites of the dimer and the tetramer are remote from one another and fully contained within the SXA protomer.

BTP and the SXA active site

Most of the direct H bonding interactions between the 21 amino acid residues of the SXA active site and BTP occur within subsite -1 (Figs. 1 and 6; Fig. 7 for BTP numbering system). With the exception of the H bond between the carboxyl group of E186 (of subsite -1) and O15 of BTP (of subsite $+1$), the remaining H bonds occur within subsite -1 : e.g., between the carboxyl group of E186 and N4 of BTP, the D14 carboxyl group and O17, the R290 guanidinium group and O19A (one orientation of O19 that shows split occupancy), the R290 guanidinium group and O17, and the T206 OH group and O19B. There are as many intramolecular H bonds (13 in all) within BTP substituents as H bonds between BTP and protein residues (Figs. 6 and 7). Additional H bonds are mediated through water molecules which serve as relays between the protein and BTP. The six water molecules of Fig. 6 occupy similar positions in all four subunits of SXA. The scarcity of H bonds between SXA subsite $+1$ residues and BTP resembles that of the catalytically inactive mutants of β -xylosidase from *G. stearothermophilus* in complex with β -1,4-xylobiose [8]. Transfer of β -1,4-xylobiose from the model of one of the mutant β -xylosidases to the model of SXA shows that BTP and β -1,4-xylobiose occupy similar space and the OH groups occupy similar positions (Fig. 7). As one might anticipate, BTP inhibits the SXA-catalyzed hydrolysis of 4NPX competitively with respect to substrate (at pH 8.0, $K_i^{\text{BTP}} = 1.25 \pm 0.03$ mM) (Fig. 8). Since BTP occupies the entire active site of SXA, there is no opportunity for forming SXA–BTP–4NPX complexes that have been seen with some monosaccharide inhibitors to present noncompetitive inhibition patterns [3].

The 1.3 Å resolution of the current structure is insufficient to resolve the protonation states of N4 and N8 of BTP (N4 of subsite -1 and N8 of subsite $+1$, Fig. 6). However, the 1.05 Å resolution of the structure of Cel5A glycoside hydrolase in complex with an imino-

Table 1
Crystallographic data collection and analysis

	Native	SeMet-SXA peak	SeMet-SXA inflection	SeMet-SXA high remote
<i>Data collection</i>				
Beamline	5 ID-B			
Spacegroup	P1	P1	P1	P1
Unit Cell <i>a</i> , <i>b</i> , <i>c</i> (Å)	77.58, 84.40, 94.04	78.41, 85.10, 94.71	78.31, 85.19, 94.71	78.51, 85.25, 94.80
α , β , γ (degrees)	78.41, 85.11, 94.71	67.65, 81.45, 75.48	67.44, 81.53, 75.50	67.59, 81.51, 75.67
Wavelength (Å)	0.9322	0.9784	0.9786	0.9632
Resolution ^a (Å)	15–1.20 (1.24–1.20)	32–1.84 (1.95–1.84)	32–1.87 (1.98–1.87)	30–1.89 (2.01–1.89)
Unique reflections	630,354 (57,143)	370,527 (61,516)	351,900 (58,586)	343,493 (56,939)
Redundancy ^b	4.48 (3.89)	1.99 (1.86)	1.99 (1.86)	1.99 (1.85)
R_{symm} ^c (%)	6.3 (38.2)	4.3 (38.0)	4.4 (38.9)	4.5 (40.8)
Completeness (%)	94.5 (91.4)	92.2 (93.3)	92.1 (93.4)	92.5 (93.5)
Average $I/\sigma I$	12.55 (3.65)	13.32 (1.79)	12.76 (1.77)	12.99 (1.75)
<i>Refinement^e</i>				
Mol/asymmetric unit	4			
Resolution ^a (Å)	15–1.3 (1.33–1.3)			
Protein atoms	17,832			
Solvent atoms	2,112			
$R_{\text{work}}/R_{\text{free}}$ ^d	13.43/16.30			
Wilson B (Å ²)	17.2			
Average B overall	11.81			
<i>Protein B-factor</i>				
A Chain	13.85			
B Chain	13.64			
C Chain	12.79			
D Chain	12.26			
Solvent B-factor	21.69			
Ligand	15.78			
<i>RMSD</i>				
Bond lengths (Å)	0.015			
Bond angles (°)	1.656			
E.S.U. (Å)	0.143			
PDB ID	3C2U			

^a Numbers in parentheses apply to the highest resolution shell.^b Anomalous pairs were not merged in processing the first three data sets listed.^c $R_{\text{symm}} = \sum (|I - \langle I \rangle|) / \sum I$ with single measurements excluded.^d $R_{\text{work}} = \sum |F_o - F_c| / \sum F_o$ and R_{free} is calculated for the 5% of data not used during refinement.^e Refinement of native data set. PDB ID 3C2U.**Table 2**
Structural comparison of GH43 β -xylosidases

β -xylosidase	PDB ID	Amino acid sequence identity to SXA (%)	C α RMSD ^a (Å)	SAS T/D/M ^b (Å ² x 10 ³)	SXA residue number (active site) ^c
SXA	3C2U	100	0.17 \pm 0.01	70.8/74.9/83.0	1111122222255 112377922588000146900 349134967446567084078 PDSFWAKFDFYEGTTHHLRFF
<i>C. acetobutylicum</i>	1YI7	70.4	0.51 \pm 0.01	72.0/75.6/83.5	PDSFWAKFDFYEGTTHHLRFF
<i>B. subtilis</i>	1YIF	63.7	0.62 \pm 0.01	72.5/75.7/83.3	PDSFWAKFDFLEGTTHHLRFF
<i>B. halodurans</i>	1YRZ	53.3	0.86 \pm 0.01	72.1/75.6/83.5	PDSFWAKFDFLEGTTHHLRFF
<i>G. stearothermophilus</i>	2EXH	61.2	0.65 \pm 0.02	71.4/74.7/82.9	PDSFWAKFDFLEGTTHHLRFF

^a Root mean square deviations between C α atoms of SXA subunit A and other β -xylosidase subunits after optimal overlays.^b Solvent accessible surface (SAS) for tetramer/dimer/monomer forms.^c Residue numbers should be read as follows: leftmost residue is 13; rightmost residue is 508.

sugar provides sufficient resolution to determine that the secondary amine is diprotonated (cationic) and that nearby carboxylic acid groups from active-site glutamates are deprotonated (anionic) forming favorable electrostatic interactions [15]. Also, in the X-ray structures of a xylanase in complex with two iminosugars, the car-

boxyl groups of the two glutamyl residues proximal to the inhibitor N groups are deprotonated at pH 7.5 (anionic) [31]. Similarly, in the SXA-BTP complex reported here, refinements were conducted with weak geometric restraints to provide unbiased positioning of atoms based on experimental data, and accurate bond lengths

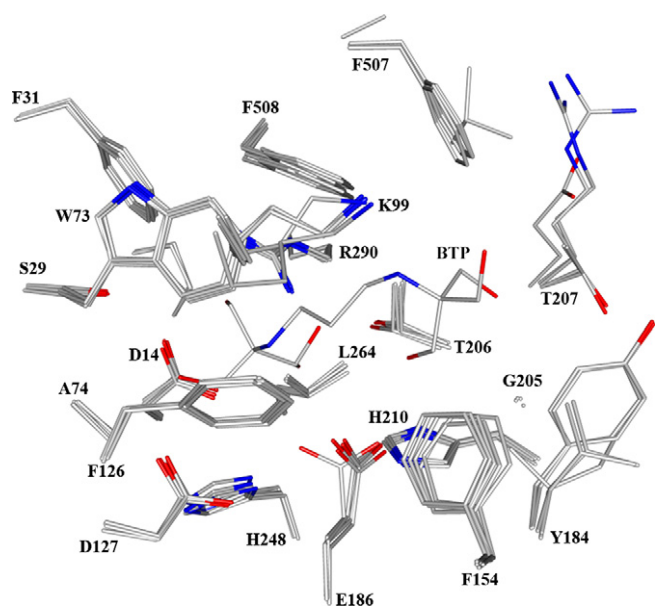


Fig. 2. Overlay of SXA active-site residues with GH43 β -xylosidases from *C. acetobutylicum*, *B. subtilis*, *B. halodurans*, and *G. stearothermophilus*. The left half comprises subsite -1; the right half comprises subsite +1. SXA has a similar orientation as Fig. 1 top panel.

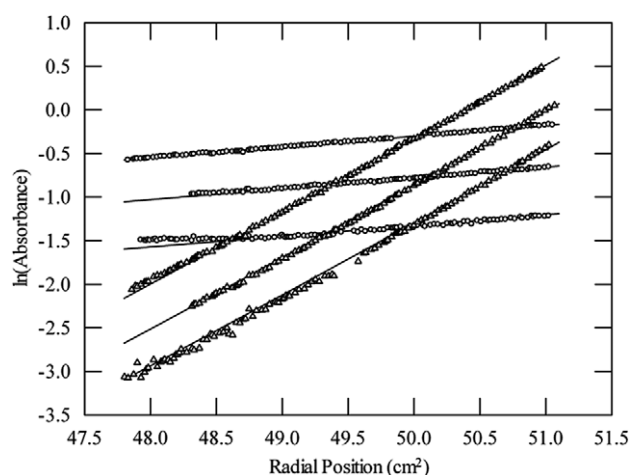


Fig. 4. Sedimentation equilibrium of SXA at pH 7.0 and 4 °C. The $\ln(\text{Absorbance})$ versus squared radial position plots are shown for the three concentrations of SXA at 3000 rpm (\circ) and 7800 rpm (Δ). Curves are based on fitting the complete data set to a model with two equilibrating species with one having twice the molecular weight of the other. Departure from linearity, more clearly seen in the 7800 rpm data, indicates the presence of more than one sedimenting species.

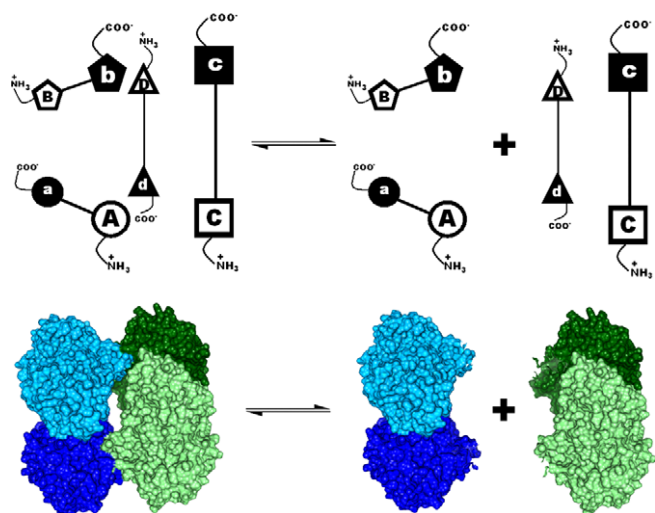


Fig. 3. Equilibrium between SXA tetramer and dimers. Top, schematic of the equilibrium. Subunits A, B, C, and D are indicated. Filled symbols indicate C-termini; and hollow symbols indicate N-termini. The homotetramer, comprising subunits A, B, C, and D is in equilibrium with two homodimers, comprising subunits A and B and C and D. Bottom, space-filled representation of equilibrium with each subunit shaded differently.

have been determined. In subunits A, B, C, and D, the C δ to O ϵ 1 bond distances of E186 are 1.24, 1.24, 1.23, and 1.25 Å, respectively, and the corresponding C δ to O ϵ 2 bond distances are 1.28, 1.28, 1.27, and 1.26 Å. The similar bond lengths reflect symmetry of charge delocalization between the O ϵ 1 and O ϵ 2 atoms of E186 and that the carboxyl group is deprotonated (anionic) under the pH 8.0 crystallization conditions. Thus, we might expect that, in the SXA-BTP complex, N4 is diprotonated (cationic) and the carboxyl group of E186 is deprotonated (anionic), which is consistent with pH profiles of $1/K_i^{\text{BTP}}$ discussed next.

Previous work, pH profiles of k_{cat}/K_m (four substrates) and $1/K_i$ (four neutral monosaccharides), has determined pK_a 5.0 (assigned to catalytic base D14) and pK_a 7.2 (assigned to catalytic acid E186)

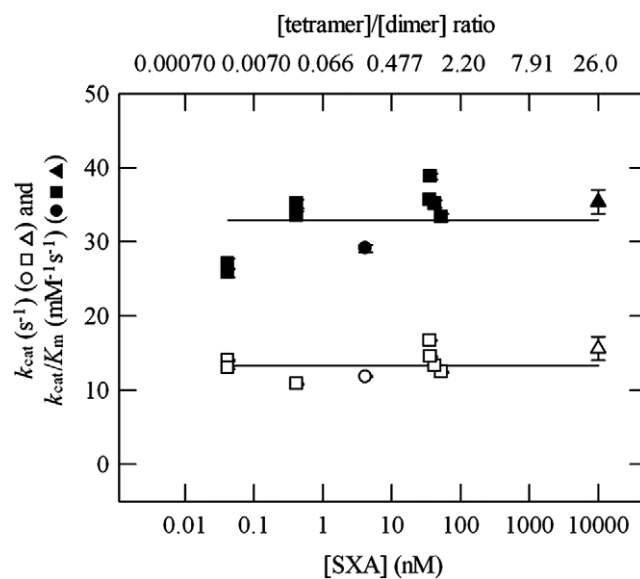


Fig. 5. Influence of SXA concentration on steady-state kinetic constants for substrate 4NPX at pH 7.0 and 25 °C. SXA concentrations of lower x axis scale are for total protomers present, regardless of quaternary state, in catalyzed reactions. For the upper x axis scale, ratios of $[\text{tetramer}]/[\text{dimer}]$ are calculated from the dissociation constant, $[\text{dimer}]^2/[\text{tetramer}] = (7.1 \pm 2.5) \times 10^{-9}$ M. Duplicate SXA reactions, containing 100 mM sodium phosphate, pH 7.0, varied concentrations of 4NPX and $I = 0.3$ M at 25 °C, were monitored at 400 nm continuously (\blacksquare , \square , \blacktriangle , \triangle) or discontinuously (\bullet , \circ) to obtain initial rates. Initial rates of reactions were fitted to Eq. (1) for determination of the displayed k_{cat} and k_{cat}/K_m values and standard errors. Reactions containing 0.04, 0.08, and 4 nM SXA were monitored 20 min, reactions containing 10000 nM SXA were monitored 0.1 s, and all other reactions were monitored for 0.3 min in determination of initial rates. Horizontal lines, indicating mean values of k_{cat} (13.3 ± 2.0 s $^{-1}$) and k_{cat}/K_m (32.9 ± 4.2 s $^{-1}$ mM $^{-1}$), are shown as visual aids. Symbols for k_{cat} and k_{cat}/K_m are defined on the left ordinate axis.

[1–3]. In a pH (6–10) profile of $1/K_i^{\text{BTP}}$, D14 would be unprotonated and we anticipated a bell-shaped dependency with pK_a 7.2 (deprotonation of E186 carboxylic acid) controlling the acidic limb and $pK_a \sim 9.5$ (deprotonation of diprotonated N4, see later for discussion of pK_a 's of BTP) controlling the basic limb. Instead, the data

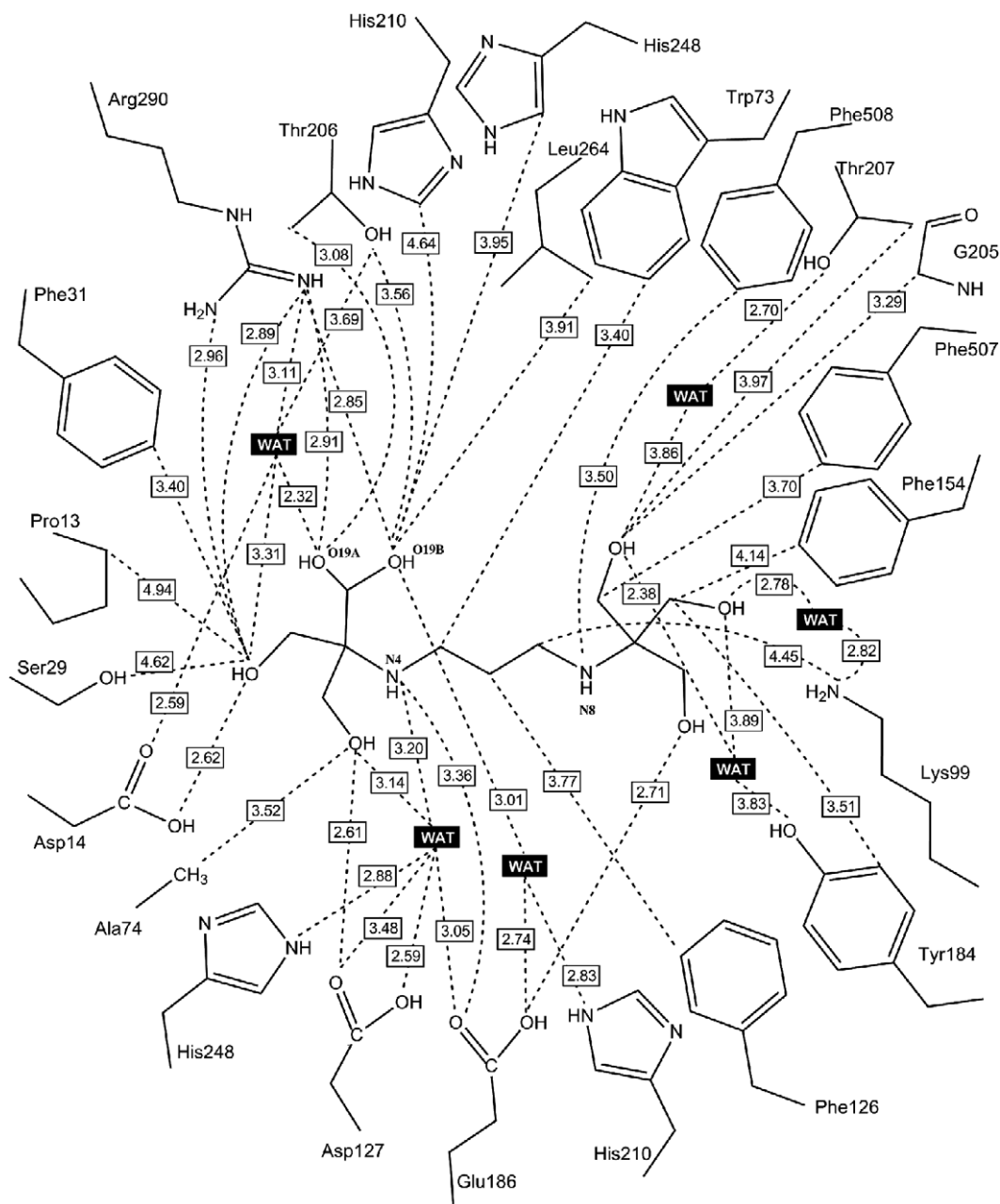


Fig. 6. Interactions between BTP and active-site residues of SXA. The 21 amino acid residues within 5 Å of BTP are shown. The left half of the schematic is subsite –1; the right half is subsite +1. The shortest distance (in Å) between each residue and BTP is indicated. Additional key distances are also indicated. SXA and BTP have similar orientations as Fig. 1 top panel and Fig. 2. WAT, the six water molecules that occupy similar positions in all four subunits of SXA.

point to three pK_a values: two controlling the acidic limb (pK_{a1} 6.8 ± 0.2 and pK_{a2} 7.8 ± 0.3) and one controlling the basic limb (pK_{a3} 9.9 ± 0.04) with a pH-independent $1/K_i^{BTP}$ $0.919 \pm 0.022 \text{ mM}^{-1}$ when the data are fitted to the model of Eq. (3) (Fig. 9a, solid line). Fitting the $1/K_i^{BTP}$ values to the model of Eq. (4) (Fig. 9a, dotted line) with single protonatable groups on the acidic and basic limbs gives larger errors in the parameter estimates and does not fit the data as well as Eq. (3) by inspection (Fig. 9a). *F* test indicates 0.18% probability that the data fit Eq. (4) as well as Eq. (3). Searching the SXA active site uncovered the possibility that a cationic N_ϵ of K99 could repel a cationic N8 of BTP, accounting for the additional pK_a 7.8. Although the N_ϵ of K99 is 5.3 Å from N8 in the model of SXA-BTP of subunit A, the side-chain bonds of K99 can be rotated out of the electron density such that the distance is shortened to below 3.7 Å.

To follow up on the possible source of pK_a 7.8, the K99A mutant of SXA was produced and purified to homogeneity. Steady-state kinetic parameters of K99A acting on 4NPX in the absence and presence of BTP are somewhat similar to those of wild-type SXA at pH 8.0 and 25 °C and indicate competitive inhibition by BTP with respect to 4NPX (Fig. S1 of Supplementary data): $k_{cat} = 9.36 \pm 0.08 \text{ s}^{-1}$, $k_{cat}/K_m = 6.71 \pm 0.047 \text{ s}^{-1} \text{ mM}^{-1}$, $K_m = 1.39 \pm 0.03 \text{ mM}$, and $K_i^{BTP} = 0.613 \pm 0.010 \text{ mM}$. The 4-fold larger k_{cat} and K_m values held by K99A relative to the wild-type enzyme are not currently understood. Also, similar to wild-type SXA, k_{cat}/K_m of K99A acting on 4NPX exhibits a bell-shaped pH dependency with pK_a 4.7 ± 0.02 and pK_a 7.3 ± 0.02 controlling the acidic and basic limbs, respectively (Fig. S2 of Supplementary data). However, mutation K99A changes the pH dependency of $1/K_i^{BTP}$ so that it has one pK_a value on each limb of the bell-shaped curve (Fig. 9b) instead

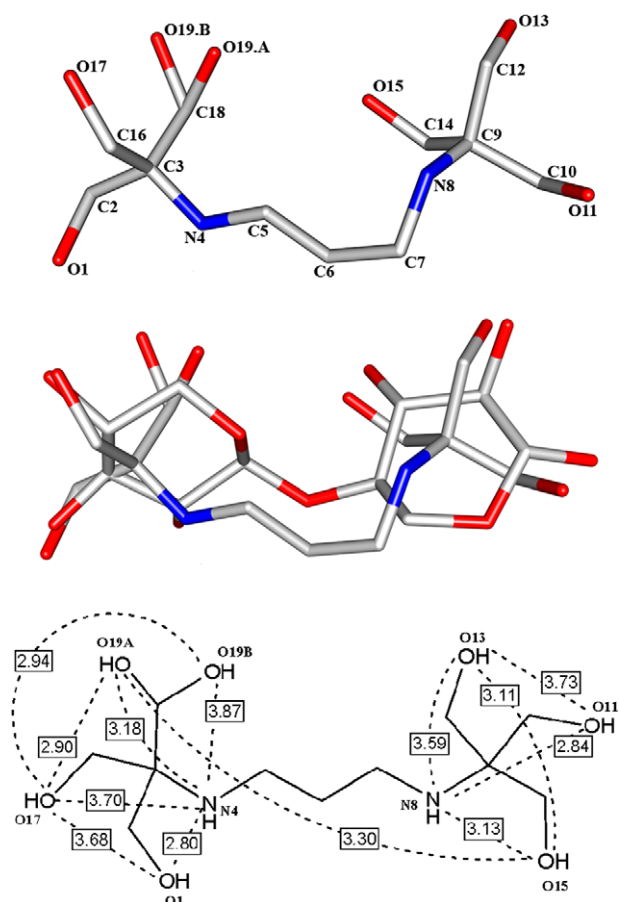


Fig. 7. 1,3-Bis[tris(hydroxymethyl)methylamino]propane (BTP) as bound to the active site of SXA. Top, numbering system. Middle, overlay of BTP with β -1,4-xylobiose from *G. stearothermophilus* (PDB ID 2EXK; containing E187G mutation of catalytic acid) was transferred to the SXA structure by overlaying C α atoms of the two proteins within 20 Å of the active-site ligands. Bottom, intramolecular H bonds.

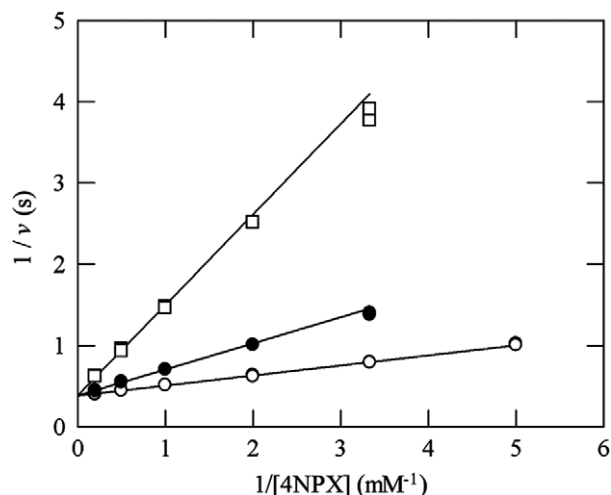


Fig. 8. Competitive inhibition of SXA-catalyzed hydrolysis of 4NPX by BTP at pH 8.0 and 25 °C. Duplicate SXA reactions, containing 0 mM (○), 2.0 mM (●) and 10.0 mM BTP (□), varied concentrations of 4NPX, 100 mM sodium phosphate, $I = 0.3$ M at pH 8.0 and 25 °C, were monitored continuously to obtain initial rates. Initial rates were fitted to Eq. (2): $k_{\text{cat}} = 2.60 \pm 0.01 \text{ s}^{-1}$, $k_{\text{cat}}/K_m = 7.94 \pm 0.15 \text{ s}^{-1} \text{ mM}^{-1}$, $K_m = 0.32 \pm 0.01 \text{ mM}$, and $K_i^{\text{BTP}} = 1.25 \pm 0.03 \text{ mM}$.

of two on the acidic limb and one on the basic limb as seen in the wild-type SXA pH profile (Fig. 9a). The $1/K_i^{\text{BTP}}$ values from K99A fit

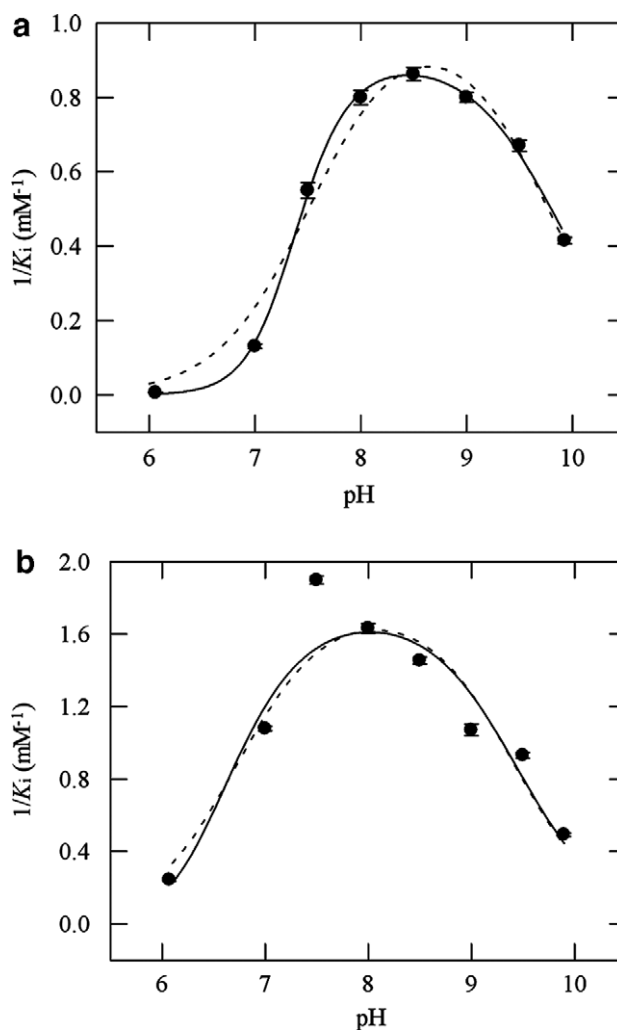


Fig. 9. Influence of pH on inhibition of SXA-catalyzed hydrolysis of 4NPX by BTP. Initial rates were determined from reactions containing varied concentrations of 4NPX and BTP at 25 °C in buffers of constant ionic strength ($I = 0.3$ M). Initial-rate data were fitted to Eq. (2) to determine K_i values at each pH; standard errors are indicated. (a) Wild-type SXA. Solid curve was generated by fitting $1/K_i$ values at each pH to Eq. (3) (three protonatable groups affecting inhibitor binding): pH-independent $1/K_i = 0.919 \pm 0.022 \text{ mM}^{-1}$, $\text{p}K_{a1} = 6.8 \pm 0.3$, and $\text{p}K_{a2} = 7.8 \pm 0.3$, and $\text{p}K_{a3} = 9.9 \pm 0.04$. Dotted curve was generated by fitting $1/K_i$ values at each pH to Eq. (4) (two protonatable groups affecting inhibitor binding): pH-independent $1/K_i = 1.02 \pm 0.07 \text{ mM}^{-1}$, $\text{p}K_{a1} = 7.5 \pm 0.1$, and $\text{p}K_{a2} = 9.8 \pm 0.1$. F test indicates 0.18% probability that data fit Eq. (4) as well as Eq. (3). (b) K99A mutant of SXA. Solid curve was generated by fitting $1/K_i$ values at each pH to Eq. (3) (three protonatable groups affecting inhibitor binding): pH-independent $1/K_i = 1.73 \pm 0.19 \text{ mM}^{-1}$, $\text{p}K_{a1} = 6.2 \pm 1.3$, $\text{p}K_{a2} = 6.6 \pm 0.4$, and $\text{p}K_{a3} = 9.4 \pm 0.2$. Dotted curve (partially hidden by solid curve) was generated by fitting $1/K_i$ values at each pH to Eq. (4) (two protonatable groups affecting inhibitor binding): pH-independent $1/K_i = 1.77 \pm 0.17 \text{ mM}^{-1}$, $\text{p}K_{a1} = 6.7 \pm 0.2$, and $\text{p}K_{a3} = 9.4 \pm 0.2$. F test indicates 64% probability that data fit Eq. (4) as well as Eq. (3).

Eq. (4) well: pH-independent $1/K_i^{\text{BTP}} = 1.77 \pm 0.17 \text{ mM}^{-1}$, $\text{p}K_{a1} = 6.7 \pm 0.2$, and $\text{p}K_{a2} = 9.4 \pm 0.2$. Fitting the data to Eq. (3), which has an additional $\text{p}K_a$ term, provides similar estimates for the parameters in Eq. (4) but a poor fit for the additional term of $\text{p}K_{a1} = 6.2 \pm 1.3$. An F test indicates a 64% probability that the data fit Eq. (4) as well as Eq. (3), indicating that the $\text{p}K_{a1}$ term is unnecessary.

Because the protonatable groups affecting binding of BTP by SXA are most likely split between enzyme and inhibitor, the pH (6–10) binding data are more correctly fitted to Eq. (5) (three protonatable groups with E186 of SXA and N8 of BTP on the acidic limb and N4 of BTP on the basic limb) and Eq. (6) (two protonatable groups with

E186 on the acidic limb and N4 on the basic limb). These equations are based on the preferred model where the dianionic ($D14^{-}E186^{-}$) SXA binds the monocationic BTP and the dicationic BTP is repelled from the wild-type SXA active site by the cationic K99 and the neutral BTP does not bind (Fig. 10). For the wild-type SXA and Eq. (5), the fitted values are pH-independent $1/K_i = 0.992 \pm 0.039 \text{ mM}^{-1}$, $pK_{a(\text{enz})} = 7.1 \pm 0.2$, and $pK_{a1(\text{inh})} = 7.1 \pm 0.2$, and $pK_{a2(\text{inh})} = 9.8 \pm 0.07$. For the wild-type SXA and Eq. (6), the fitted values are pH-independent $1/K_i = 1.02 \pm 0.08 \text{ mM}^{-1}$, $pK_{a(\text{enz})} = 7.5 \pm 0.1$, and $pK_{a(\text{inh})} = 9.8 \pm 0.1$. An *F* test indicates 8.6% probability that data fit Eq. (6) as well as Eq. (5), which is borderline supportive of Eq. (5) over Eq. (6). It should be noted that the 8.6% probability value com-

pare fitting data to the entire Eq. (5) and Eq. (6). When constants replace parameters ($pK_{a(\text{enz})} = 7.2$ and $pK_{a2(\text{inh})} = 9.8$) and Eqs. (5) and (6), fitting the data to Eq. (5) determines $pK_{a1(\text{inh})} = 7.0 \pm 0.1$ and the *F* test indicates 0.09% probability that the data fit Eq. (6) as well as Eq. (5). The 0.09% probability indicates that the $pK_{a1(\text{inh})}$ term of Eq. (5) (the additional pK_a on the acidic limb) is strongly required for fitting the wild-type data. Similar treatment of the other models considered here (three models represented by Eqs. (3) and (4), Eqs. (5) and (6), and Eqs. (7) and (6)) also provides low *F* test probabilities that the wild-type data fit equations without the additional pK_a on the acidic limb as well as to equations that contain the term. In no case is the additional pK_a term required to fit the K99A mutant data. It should also be noted that when there are two pK_a terms describing the acidic limb, accurate determinations of the values for individual pK_a terms can require data for more pH values than provided here, particularly when the pK_a values are close together. For the K99A SXA and Eq. (5), the fitted values are pH-independent $1/K_i = 1.72 \pm 0.01 \text{ mM}^{-1}$, $pK_{a(\text{enz})} = 6.6 \pm 0.02$, and $pK_{a1(\text{inh})} = 5.9 \pm 0.06$, and $pK_{a2(\text{inh})} = 9.4 \pm 0.01$. For the K99A SXA and Eq. (6), the fitted values are pH-independent $1/K_i = 1.77 \pm 0.17 \text{ mM}^{-1}$, $pK_{a(\text{enz})} = 6.7 \pm 0.2$, and $pK_{a(\text{inh})} = 9.4 \pm 0.2$. *F* test indicates 45% probability that data fits Eq. (6) as well as Eq. (5), indicating that the term ($pK_{a1(\text{inh})} = 5.9$) is unnecessary for describing the K99A SXA pH dependency. Titration of 10 mM BTP with 1 N HCl and using a pH electrode provides pK_a values of 6.92 ± 0.01 and 9.16 ± 0.01 in water and 7.07 ± 0.02 and 9.19 ± 0.01 in 0.3 M NaCl. So in the model of Eq. (5) with wild-type SXA data, $pK_{a(\text{enz})} 7.1$ is assigned to E186, $pK_{a1(\text{inh})} 7.1$ is assigned to N8 of BTP (the N of subsite +1, Fig. 6), and $pK_{a2(\text{inh})} 9.8$ is assigned to N4 of BTP (the N of subsite -1, Fig. 6). In the model, K99 is assumed to be cationic throughout the pH (6–10) titration. $pK_{a(\text{enz})} 7.1$ is similar to $pK_a 7.2$ determined from k_{cat}/K_m pH titration [1]. $pK_{a1(\text{inh})} 7.1$ is similar to the solution $pK_a 7.07$ determined for N8 of BTP. $pK_{a2(\text{inh})} 9.8$ is raised from its solution $pK_a 9.19$. Raising the pK_a of BTP from its solution value of 9.19 to its enzyme value of 9.8 is likely due to the anionic environment of subsite -1 of SXA. Thus, the pK_a values of the model can be fully accounted for.

Another model that can be considered is that in which the extra pK_a seen on the acidic limb of Fig. 9a reports K99 of SXA. This model is tempting because, as seen above, wild-type SXA does not bind dicationic BTP, but the K99A mutant SXA does. ($D14^{-}E186^{-}$) SXA binds the monocationic BTP and the dicationic BTP is repelled from the wild-type SXA active site when K99 becomes cationic and the neutral BTP does not bind. This model is evaluated through Eq. (7) (three protonatable groups with E186 and K99 of SXA on the acidic limb and N4 of BTP on the basic limb) and Eq. (6) (two protonatable groups with E186 on the acidic limb and N4 on the basic limb) (Fig. S3 of Supplementary data). For the wild-type SXA and Eq. (7), the fitted values are pH-independent $1/K_i = 0.919 \pm 0.023 \text{ mM}^{-1}$, $pK_{a1(\text{enz})} = 7.8 \pm 0.3$, and $pK_{a2(\text{enz})} = 6.8 \pm 0.3$, and $pK_{a(\text{inh})} = 9.9 \pm 0.04$. For the wild-type SXA and Eq. (6), the fitted values are pH-independent $1/K_i = 1.02 \pm 0.08 \text{ mM}^{-1}$, $pK_{a(\text{enz})} = 7.5 \pm 0.1$, and $pK_{a(\text{inh})} = 9.8 \pm 0.1$. An *F* test indicates 0.18% probability that data fit Eq. (6) as well as Eq. (7), indicating that the term ($pK_{a1(\text{enz})} = 7.8$) is necessary in describing the wild-type SXA pH dependency. For the K99A SXA and Eq. (7), the fitted values are pH-independent $1/K_i = 1.73 \pm 0.19 \text{ mM}^{-1}$, $pK_{a1(\text{enz})} = 6.2 \pm 1.3$, and $pK_{a2(\text{enz})} = 6.6 \pm 0.4$, and $pK_{a(\text{inh})} = 9.4 \pm 0.2$. For the K99A SXA and Eq. (6), the fitted values are pH-independent $1/K_i = 1.77 \pm 0.17 \text{ mM}^{-1}$, $pK_{a(\text{enz})} = 6.7 \pm 0.2$, and $pK_{a(\text{inh})} = 9.4 \pm 0.2$. *F* test indicates 64% probability that data fits Eq. (6) as well as Eq. (5), indicating that the term ($pK_{a1(\text{enz})} = 6.2$) is unnecessary for describing the pH dependency of K99A SXA. As can be seen from fitting the data to Eqs. (7) and (6), the resulting values for the parameters are similar to those obtained when the data were fitted to Eqs. (3) and (4). From the fit of wild-type SXA data to Eq. (7), $pK_{a1(\text{enz})} 7.8$ is assigned to K99,

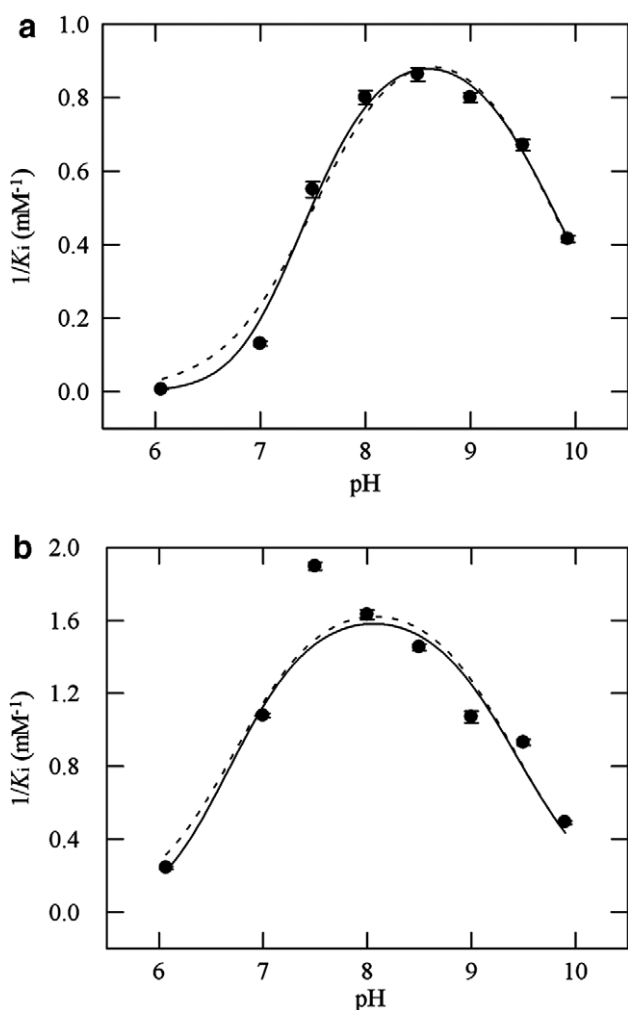


Fig. 10. Influence of pH on inhibition of SXA-catalyzed hydrolysis of 4NPX by BTP. Initial rates were determined from reactions containing varied concentrations of 4NPX and BTP at 25 °C in buffers of constant ionic strength ($I = 0.3 \text{ M}$). Initial-rate data were fitted to Eq. (2) to determine K_i values at each pH; standard errors are indicated. (a) Wild-type SXA. Solid curve was generated by fitting $1/K_i$ values at each pH to Eq. (5) (three protonatable groups affecting inhibitor binding): pH-independent $1/K_i = 0.992 \pm 0.039 \text{ mM}^{-1}$, $pK_{a(\text{enz})} = 7.1 \pm 0.2$, and $pK_{a1(\text{inh})} = 7.1 \pm 0.2$, and $pK_{a2(\text{inh})} = 9.8 \pm 0.07$. Dotted curve was generated by fitting $1/K_i$ values at each pH to Eq. (6) (two protonatable groups affecting inhibitor binding): pH-independent $1/K_i = 1.02 \pm 0.08 \text{ mM}^{-1}$, $pK_{a(\text{enz})} = 7.2 \pm 0.1$, and $pK_{a(\text{inh})} = 9.8 \pm 0.1$. *F* test indicates 8.6% probability that data fit Eq. (6) as well as Eq. (5). (b) K99A mutant of SXA. Solid curve was generated by fitting $1/K_i$ values at each pH to Eq. (5) (three protonatable groups affecting inhibitor binding): pH-independent $1/K_i = 1.72 \pm 0.01 \text{ mM}^{-1}$, $pK_{a(\text{enz})} = 6.6 \pm 0.02$, and $pK_{a1(\text{inh})} = 5.9 \pm 0.06$, and $pK_{a2(\text{inh})} = 9.4 \pm 0.01$. Dotted curve (partially hidden by solid curve) was generated by fitting $1/K_i$ values at each pH to Eq. (6) (two protonatable groups affecting inhibitor binding): pH-independent $1/K_i = 1.77 \pm 0.17 \text{ mM}^{-1}$, $pK_{a(\text{enz})} = 6.7 \pm 0.2$, and $pK_{a(\text{inh})} = 9.4 \pm 0.2$. *F* test indicates 45% probability that data fit Eq. (6) as well as Eq. (5).

$pK_{a2(\text{enz})}$ 6.8 is assigned to E186, and $pK_{a(\text{inh})}$ 9.9 is assigned to N4 of BTP. Lowering the pK_a value of the N_ϵ of lysine from its solution value of 10.4 to its enzyme value of 7.8 could be due to the hydrophobic environment of subsite +1 of SXA. Perturbation of pK_a values to near 7.8 and below for the N_ϵ group of lysine residues in enzymes, are documented in the literature: e.g., pK_a 7.9 for the active-site K166 of ribulose1,5-bisphosphate carboxylase/oxygenase [32] and pK_a 6.0 for the active-site lysine of acetoacetate decarboxylase [33]. $pK_{a2(\text{enz})}$ 6.8 is similar to pK_a 7.2 assigned to E186 from the pH dependency of k_{cat}/K_m [1]. As stated above, raising the pK_a of N4 of BTP from its solution pK_a 9.19 to its enzyme pK_a 9.9 is likely due to the anionic environment of subsite –1 of SXA. A weakness in this model is that the pK_a of N8 of BTP is unaccounted for. The model requires the pK_a of N8 to be above 7.8 so that BTP is dicationic and repelled by K99 when the lysyl N_ϵ group becomes cationic ($pK_{a1(\text{enz})} = 7.8$).

Summary and conclusion

The close correspondence of the relative positions of active-site residues of SXA and the β -xylosidase from *G. stearothermophilus* is important because the structure of the latter enzyme in complex with β -1,4-xylobiose has previously been used for analyzing the effects of site-directed mutations of SXA on catalysis and substrate recognition, including the mutations that change relative substrate specificities (k_{cat}/K_m)^{4NPX}/ (k_{cat}/K_m) ^{4NPA} with implications for substrate distortion in approaching the transition states [4]. The similar positioning of active-site residues among the five GH43 β -xylosidases (Fig. 2) underscores the rigidity noted for the 5-bladed propeller domains [9], which house most of the active-site residues.

The stability of the SXA tertiary structure is apparently not shared by the SXA quaternary structure. The K_d [dimer]²/[tetramer] of 7.1×10^{-9} M determined here indicates that under ordinary reaction conditions at pH 7.0 and 25 °C with 0.3 min monitoring of initial rates, the dimer/tetramer ratio hovers around one. It is reassuring to know that the ratio can increase or decrease to a considerable degree, as may occur in temperature or pH studies, for example, without affecting steady-state kinetic constants. The stability of the catalytic parameters is undoubtedly due, in part, to the spatial separation of the active sites within the tetramers and the complete enclosure of the individual active sites within the protomers.

BTP provides the first example of an SXA inhibitor that binds only to the catalytically inactive, dianionic (D14[–]E186[–]) form of SXA. The monocationic form of BTP binds to wild-type SXA, while both mono- and di-cationic forms of BTP can bind to K99A SXA. Four inhibitory monosaccharides and three substrates (4NPX, β -1,4-xylobiose and β -1,4-xylotriose) bind to both the catalytically active, monoanionic (D14[–]E186^H) form of SXA and the D14[–]E186[–] SXA [1–3]. The 4NPA substrate is the only ligand that appears to bind exclusively to D14[–]E186^H SXA. BTP occupies both subsites of the SXA active site so it cannot serve as a probe for the ability of other SXA inhibitors to bind to subsite +1 when subsite –1 of D14[–]E186[–] is occupied by BTP. In contrast, two monosaccharides have been shown to bind the active site of D14[–]E186^H SXA nonexclusively and simultaneously [3]. However, the example of BTP binding with its cationic N4 group occupying subsite –1 and its cationic N8 group repelled from binding to subsite +1 suggests that smaller aminoalcohols could serve as probes that occupy only subsite –1 of D14[–]E186[–] SXA; and this will be examined in a future study.

Acknowledgments

We thank Jay D. Braker for excellent technical assistance. Sedimentation equilibrium data was collected in Biophysics Instrumentation Facility at the University of Wisconsin (Madison), which was established with support from the University of Wisconsin, and Grants BIR-9512577 (NSF) and S10 RR13790 (NIH). This work was supported by USDA funding of CRIS 3620-41000-118-00D. The mention of firm names or trade products does not imply that they are endorsed or recommended by the U.S. Department of Agriculture over other firms or similar products not mentioned.

Appendix A. Supplementary data

Supplementary data associated with this article can be found, in the online version, at doi:10.1016/j.abb.2008.03.007.

References

- [1] D.B. Jordan, X.-L. Li, C.A. Dunlap, T.R. Whitehead, M.A. Cotta, Appl. Biochem. Biotechnol. 141 (2007) 51–76.
- [2] D.B. Jordan, Appl. Biochem. Biotechnol. 146 (2008) 137–149.
- [3] D.B. Jordan, J.D. Braker, Arch. Biochem. Biophys. 465 (2007) 231–246.
- [4] D.B. Jordan, X.-L. Li, Biochem. Biophys. Acta 1774 (2007) 1192–1198.
- [5] D.B. Jordan, X.-L. Li, C.A. Dunlap, T.R. Whitehead, M.A. Cotta, Appl. Biochem. Biotechnol. 137–140 (2007) 93–104.
- [6] K.A. Gray, L. Zhao, M. Emptage, Curr. Opin. Chem. Biol. 10 (2006) 141–146.
- [7] B.S. Dien, N.N. Nichols, P.J. O'Bryan, R.J. Bothast, Appl. Biochem. Biotechnol. 84–86 (2000) 181–196.
- [8] C. Br ux, A. Ben-David, D. Shallom-Shezif, M. Leon, K. Niefind, G. Shoham, Y. Shoham, D. Schomburg, J. Mol. Biol. 359 (2006) 97–109.
- [9] V. F l p, D.T. Jones, Curr. Opin. Struct. Biol. 9 (1999) 715–721.
- [10] D. Nurizzo, J.P. Turkenburg, S.J. Charnock, S.M. Roberts, E.J. Dodson, V.A. McKie, E.J. Taylor, H.J. Gilbert, G.J. Davies, Nat. Struct. Biol. 9 (2002) 665–668.
- [11] J. Sevcik, A. Solovicov , E. Hostenov , J. Gasperik, K.S. Wilson, Z. Dauter, Acta Crystallogr. D54 (1998) 854–866.
- [12] N. Ramasubbu, K. Sundar, C. Raguath, M.M. Rafi, Arch. Biochem. Biophys. 421 (2004) 115–124.
- [13] T.M. Gloster, P. Meloncelli, R.V. Stick, D. Zechel, A. Vasella, G.J. Davies, J. Am. Chem. Soc. 129 (2007) 2345–2354.
- [14] D.L. Zechel, A.B. Boraston, T. Gloster, C.M. Boraston, J.M. Macdonald, D.M. Tilbrook, R.V. Stick, G.J. Davies, J. Am. Chem. Soc. 125 (2003) 14313–14323.
- [15] A. Varrot, C.A. Tarling, J.M. Macdonald, R.V. Stick, D.L. Zechel, S.G. Withers, G.J. Davies, J. Am. Chem. Soc. 125 (2003) 7496–7497.
- [16] E.F. Pettersen, T.D. Goddard, C.C. Huang, G.S. Couch, D.M. Greenblatt, E.C. Meng, T.E. Ferrin, J. Comput. Chem. 25 (2004) 1605–1612.
- [17] T.R. Whitehead, M.A. Cotta, Curr. Microbiol. 43 (2001) 293–298.
- [18] S. Doubl , Methods Enzymol. 276 (1997) 523–530.
- [19] A. Howard, Data processing in macromolecular crystallography, in: P.E. Bourne, K.D. Watenpaugh (Eds.), Crystallographic Computing 7: Proceedings from the Macromolecular Crystallographic Computing School, 1996, Oxford University Press, Oxford, 2000. Available from: <http://www.sdsc.edu/Xtal/IUCr/CC/School96/IUCr.html>.
- [20] W. Kabsch, J. Appl. Cryst. 26 (1993) 795–800.
- [21] C.M. Weeks, R. Miller, J. Appl. Cryst. 32 (1999) 120–124.
- [22] Z. Otwinowski, in: W. Wolf, P.R. Evans, A.G.W. Leslie (Eds.), Proceedings of the CCP4 Study Weekend, SERC Daresbury Laboratory, 1991, Warrington, UK, pp. 80–86.
- [23] K. Cowtan, Joint CCP4 and ESF-EACBM Newsletter on Protein Crystallography 31 (1994) 34–38.
- [24] A. Perrakis, R. Morris, V.S. Lamzin, Nat. Struct. Biol. 6 (1999) 458–463.
- [25] D.E. McRee, J. Struct. Biol. 125 (1999) 156–165.
- [26] P. Emsley, K. Cowtan, Acta Cryst. D60 (2004) 2126–2132.
- [27] G.N. Murshudov, A. Lebedev, A.A. Vagin, K.S. Wilson, E.J. Dodson, Acta Cryst. D55 (1999) 247–255.
- [28] S.C. Gill, P.H. von Hippel, Anal. Biochem. 182 (1989) 319–326.
- [29] T.M. Laue, Methods Enzymol. 259 (1995) 427–452.
- [30] R.J. Leatherbarrow, Grafit Version 5, Eritacus Software Ltd., Horley, U.K., 2001.
- [31] T.M. Gloster, S.J. Williams, S. Roberts, C.A. Tarling, J. Wicki, S.G. Withers, G.J. Davies, Chem. Commun. (2004) 1794–1795.
- [32] F.C. Hartman, S. Milanez, E.H. Lee, J. Biol. Chem. 260 (1985) 13968–13975.
- [33] F.C. Kokesh, F.H. Westheimer, J. Am. Chem. Soc. 93 (1971) 7270–7274.